DOI: 10.1002/cbic.200700416

Plasmonic Magnetic Nanostructure for Bimodal Imaging and Photonic-Based Therapy of Cancer Cells

Yong Taik Lim,[a] Mi Young Cho,[a] Jin Kyeong Kim,[a] Seol Hwangbo,[b] and Bong Hyun Chung*[a]

Nanomaterials that contain two or more different functionalities are attractive candidates for technological applications in the areas of biology and medicine.[1–9] Among a variety of nanoparticles, magnetic nanoparticles offer exciting new opportunities for improvements in the quality of magnetic resonance imaging (MRI), hyperthermia treatment for malignant cells, site-specific drug delivery, and the manipulation of cells. Iron oxide magnetic nanoparticles (Fe_2O_3 and Fe_3O_4), in particular, have attracted great interest in the areas of biomedicine and biology due to their inherent biocompatibility.[10–14] Superparamagnetic iron oxide nanoparticles have been extensively studied for use as MRI contrast agents because in the presence of an external magnetic field, a magnetic field is induced within these nanoparticles that polarizes the spins of neighboring water protons; this results in enhanced contrast in the final image.[15–18] In addition to their biocompatibility, the strong light-absorption and scattering properties of the gold nanostructures, which is due to the surface plasmon resonance effect are also being investigated and have been proposed for a variety of types of applications such as optical sensors, imaging contrast agents, targeted cancer therapy and photothermal triggers for drug release.[2,19–30] Several previous studies have shown that by controlling the structure of these nanoparticles, for example, core-shell, hollow or nanorod-like structures, the optical resonance wavelength of gold nanoparticles can be tuned to the near-infrared (NIR, in the range of 750 to 1200 nm) region of the spectrum, where the light transmission through biological tissues is known to be quite high.[23,31,32] Hence, a combination of the distinct optical characteristics of gold nanostructures in the NIR region of the spectrum with the multifunctional properties of magnetic nanoparticles offers a great potential in biomedical applications for the future.

We have designed novel nanocomposite particles that consist of hollow-type gold nanoshells with iron oxide nanoparticles inside their interiors. These types of nanocomposite particles were especially designed to be used as multifunctional nanoplatforms for biomedical imaging and targeted cancer therapy. The iron oxide nanoparticles have a magnetic character that enables them to be used as contrast agents for MRI, whereas the hollow-type gold nanostructures, which encapsulate the magnetic nanoparticles provide strong absorption (and/or scattering) of NIR light. These novel nanostructures were used as a bimodal contrast agents for MRI and scattering-based optical imaging. We further extended their application for the selective destruction of breast cancer cells (SKBR3) by using a photothermal effect.

Scheme 1 depicts the synthetic scheme of multifunctional nanocomposite particles for molecular imaging and targeted cancer therapy. The TEM images of nanocomposite particles are shown in Figure 1. The final structure is a hollow-type gold nanoshell that contains magnetic nanoparticles within their interiors. We synthesized monodisperse iron oxide nanoparticles (Fe_3O_4, 9–11 nm; Figure 1A) in an organic solvent, then deposited the gold nanolayers on these magnetic nanoparticles.[33] The thickness of the outer Au nanolayer in the gold-coated Fe_3O_4 (Fe_3O_4@Au) nanoparticles that was determined from TEM image analysis, was about 2–3 nm (Figure 1B). The synthesized gold-coated magnetic nanoparticles were sequentially coated with silver for a subsequent replacement reaction.[34,35] The thickness of the silver nanolayer was controlled by the mixing

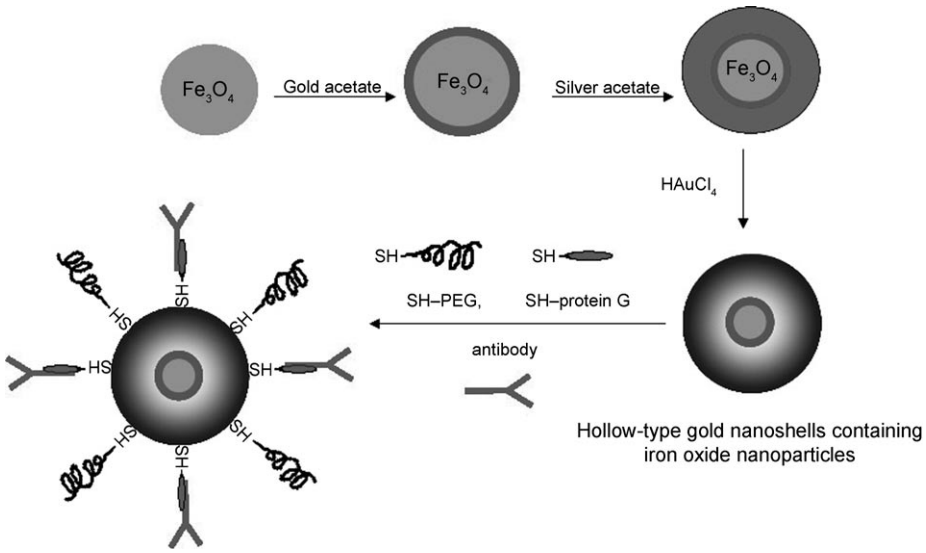

Scheme 1. Overview of the preparation of the iron-oxide-containing nanoshells and the antibody-coated nanoshells.

[a] *Dr. Y. T. Lim, M. Y. Cho, J. K. Kim, Dr. B. H. Chung*
BioNanotechnology Research Center
Korea Research Institute of Bioscience and Biotechnology
Daejeon 305-806 (South Korea)
Fax: (+82) 42-879-8594
E-mail: chungbh@kribb.re.kr

[b] *Dr. S. Hwangbo*
Department of Radiology, Daejeon St. Mary's Hospital
The Catholic University of Korea
Daejeon 305-806 (South Korea)

Supporting information for this article is available on the WWW under http://www.chembiochem.org or from the author.

WILEY InterScience DISCOVER SOMETHING GREAT
© 2007 Wiley-VCH Verlag GmbH & Co. KGaA, Weinheim

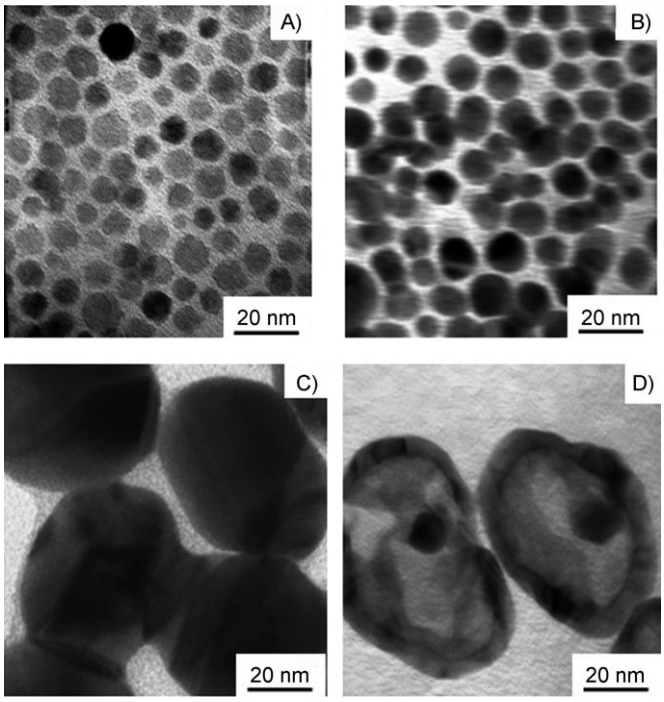

Figure 1. TEM images of A) iron oxide nanoparticles (Fe_3O_4), B) gold-coated iron oxide nanoparticles (Fe_3O_4@Au), C) silver-coated Fe_3O_4@Au, and D) gold nanoshells that contain gold-coated iron oxide nanoparticles (HGNS-(Fe_3O_4@Au)).

ratio of silver acetate and the Fe_3O_4@Au nanoparticles. By adding more silver acetate to the silver-coated Fe_3O_4@Au nanoparticles, we were able to control the growth of the outer silver layer (Figure 1C). Furthermore, because we intended to use the outer silver layer as a template for the formation of hollow gold nanoshells, we systematically controlled and varied the final thickness of the silver layer by considering the optical resonance peak of the final gold nanoshells (data not shown). As a typical example, we have synthesized hollow-type gold nanoshells that contain Fe_3O_4@Au (hereafter, HGNS-(Fe_3O_4@Au)) within their interiors, whose optical resonance peak reside around the NIR region of spectrum (see the Experimental Section for details). After synthesizing silver-coated Fe_3O_4@Au nanoparticles, they were transformed into hollow-type gold nanostructures by means of a replacement reaction between a chloroauric acid ($HAuCl_4$) solution and the outer silver layer in the silver-coated Fe_3O_4@Au nanoparticles. As seen from the TEM image in Figure 1D, the Fe_3O_4@Au nanoparticles reside in the core of the hollow-type gold nanoshells. In the final step, we have modified the surface of the nanocomposite particles with monoclonal antibodies (anti-HER2) that can target epidermal growth factor receptors (EFGR); EFGRs are overexpressed on the surface of breast cancer cells (SKBR3). Further, we used polyethylene glycol (PEG) moieties to increase the water solubility and to block nonspecific interactions (Scheme 1).[25] In particular, we used protein G molecules to optimize the orientation of the antibodies on the surface of the gold nanoshells.[36]

To monitor the structural changes that took place during the preparation of the HGNS(Fe_3O_4@Au), we used a UV/Vis–NIR spectrophotometer (Figure 2). When a gold nanolayer was formed on the surface of the Fe_3O_4 nanoparticles, we observed an optical resonance peak at around 600 nm (Figure 2A–C).

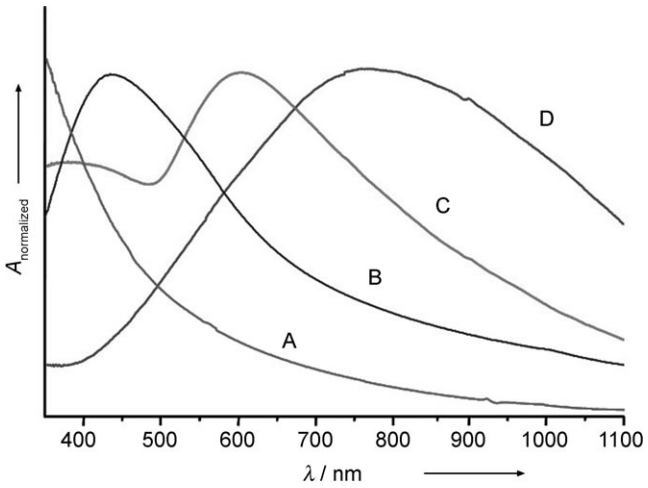

Figure 2. UV/Vis–NIR spectrum of A) Fe_3O_4, B) silver-coated Fe_3O_4@Au, C) Fe_3O_4@Au, and D) HGNS(Fe_3O_4@Au).

Compared to the resonance wavelength of bare gold nanoparticles (at around 520 nm), the resonance peak in the case of these nanocomposite particles, exhibited a shift to a longer wavelength. This shift can result from a change in the dielectric environment, as has been reported in previous studies.[37,38] The optical resonance peak of metal-coated nanoparticles can be determined by the thickness ratio of the core and the shell as well as by the dielectric constant of each component. When silver acetate reacted with the Fe_3O_4@Au nanoparticles, the resonance wavelength was observed in the 440 nm region; this suggests that a thick silver layer had formed on the surface of the Fe_3O_4@Au nanoparticles (Figure 2B and C). After systematically controlling the thickness of the outer silver layer by repeated experiments, we found that under the optimized conditions, the high optical absorption of the hollow-type gold nanoshells (after the replacement reaction) existed at around 808 nm (the wavelength of NIR laser). The optical resonance peak shifted to the 770 nm region when the $HAuCl_4$ solution was added (Figure 2B–D); this indicates the formation of hollow-type gold nanoshells. Due to the broad absorption spectrum as seen in Figure 2D, the optical absorption density of the hollow-type gold nanoshells at 808 nm was similar to that at 770 nm.

The potential of the synthesized nanocomposite particles HGNS(Fe_3O_4@Au) for biomedical imaging and targeted cancer therapy were investigated in detail. Iron oxide nanoparticles that are encapsulated by the hollow-type gold nanoshells can be used as a contrast agent for MRI, while the hollow-type gold nanoshells provide strong absorption (scattering) of NIR light. HGNS(Fe_3O_4@Au) exhibited superparamagnetic characteristics (Figure 3A) and was found to generate MR contrast signals (see Figure S1 in the Supporting Information). The satura-

 © 2007 Wiley-VCH Verlag GmbH & Co. KGaA, Weinheim

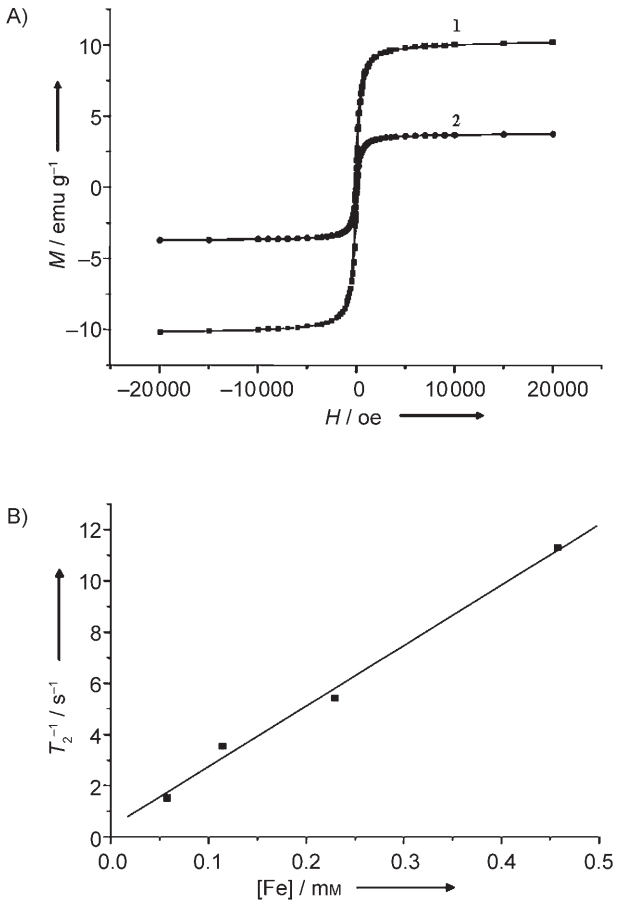

Figure 3. Magnetic properties of HGNS(Fe_3O_4@Au). A) Magnetization (M) hysteresis for Fe_3O_4@Au (sample 1) and HGNS(Fe_3O_4@Au) (sample 2) at 300 K, B) the spin–spin relaxation rates of HGNS(Fe_3O_4@Au).

tion moment per unit mass, M_S, at 10 kOe was 3.70 emu g^{-1} for HGNS(Fe_3O_4@Au) and 9.95 emu g^{-1} for Fe_3O_4@Au. The decrease in the M_S of HGNS(Fe_3O_4@Au), compared to that of iron oxide nanoparticles (59.3 emu g^{-1}), might be due to the large volume of the gold nanoshells that encapsulate the iron oxide nanoparticles. The increase in the concentration of nanoparticles leads to a dramatic decrease in signal intensity due to the shortening of T_2 (Figure S1). The relaxivity (R_2) of the HGNS(Fe_3O_4@Au), which is a measure of the change in the spin–spin relaxation rate ($1/T_2$) per unit concentration, was 23.61 mM^{-1} s^{-1} (Figure 3B). Because HGNS(Fe_3O_4@Au) contains only one Fe_3O_4@Au within its interior, the relaxivity value is lower than that of the previous reported values in which multiple iron oxide nanoparticles were bound to silica nanoparticles. However HGNS(Fe_3O_4@Au) does not contain silica materials in the core part. The HGNS(Fe_3O_4@Au) is only composed of biocompatible hollow gold nanostructure and iron oxide nanoparticles. Furthermore, we could easily tune the optical resonance peak of the hollow gold nanostructure just by controlling the shell thickness; this is different from previous studies,[2] in which the optical resonance of the composite nanoparticles was controlled by the relative thickness of a silica core and gold shell.

We have further investigated whether the HGNS(Fe_3O_4@Au) could be used in targeted imaging and therapy of cancer cells. The HGNS(Fe_3O_4@Au) were conjugated with monoclonal antibodies (anti-HER2) that can target epidermal growth factor receptors (EFGR), one of which is HER2 (human epidermal growth factor receptor 2); this is often overexpressed on the surface of breast cancer cells.[25] To investigate the specificity of HGNS(Fe_3O_4@Au)/anti-HER2, HER2-positive breast cancer cells (SKBR3, 2.5×10^5) and HER2-negative breast cancer cells (MCF7, 2.5×10^5) were prepared. To visualize the attachment of HGNS(Fe_3O_4@Au)/anti-HER2 on the surface of cell line, anti-rabbit IgG tetramethyl rhodamine iso-thiocyanate (TRITC) was also conjugated to HGNS(Fe_3O_4@Au)/anti-HER2 in the antibody conjugation step. As shown in Figure 4, strong TRITC fluorescence was only observed in the HER2-positive SKBR3 breast cancer cells. The attachment of HGNS(Fe_3O_4@Au)/anti-HER2 onto the SKBR3 cells, suggests that there is a specific interaction between the anti-HER2 that bound to HGNS(Fe_3O_4@Au) and HER2, which is overexpressed on the SKBR3 cells. Based on these experimental results, we have further explored whether HGNS(Fe_3O_4@Au)/anti-HER2 could be used for molecular imaging and therapy of SKBR3 breast cancer cells. Figure 5A shows the T_2-weighted images (TR = 4000 and TE = 120) of SKBR3 cells that had been labelled with HGNS(Fe_3O_4@Au)/anti-HER2. The decrease in the magnetic resonace (MR) signal intensity (darkening) is due to the presence of HGNS(Fe_3O_4@Au)/anti-HER2 (0.45 mM Fe) on the surface of SKBR3 cells. In addition to being used in MR-based cellular imaging, HGNS(Fe_3O_4@Au)/anti-HER2 can also be used as optical imaging contrast agents for the diagnosis of breast cancer. Due to the strong surface-plasmon-enhanced scattering properties of metal nanoparticles, the HGNS(Fe_3O_4@Au)/anti-HER2, which are targeted to SKBR3 cells can be clearly detected with a dark-field microscope (Figure 5B).[39] The data showed that the HGNS(Fe_3O_4@Au)/anti-HER2 can be used as bimodal imaging agents for breast cancer diagnosis, particularly with the techniques of

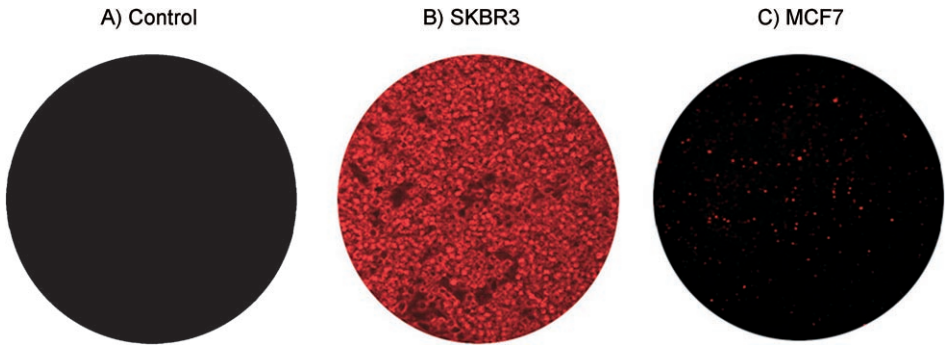

Figure 4. A) Fluorescence image of SKBR3 cells only, B) SKBR3 cells that were incubated with HGNS(Fe_3O_4@Au)/anti-HER2, and C) MCF cells that were incubated with HGNS(Fe_3O_4@Au)/anti-HER2. For the fluorescence image, anti-rabbit IgG (TRITC) was also conjugated on the HGNS(Fe_3O_4@Au)/anti-HER2.

 © 2007 Wiley-VCH Verlag GmbH & Co. KGaA, Weinheim

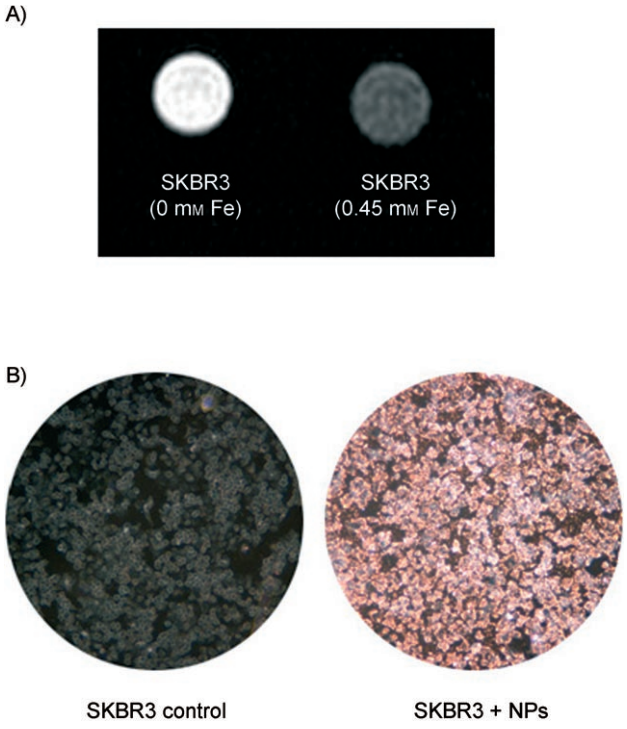

Figure 5. Imaging of SKBR3 cells that were targeted with HGNS(Fe_3O_4@Au)/anti-HER2. A) an MR image, B) a dark-field scattering image.

MRI (as shown in Figure 5A) and optical imaging (as shown in Figure 5B). One of the merits of using gold nanostructures as chromophores is that they have non-bleaching properties in cellular imaging. Although fluorescent semiconductor nanocrystals are considered to be an alternative solution to the photobleaching problems of organic dyes, there are still toxicity issues that need to be resolved.[32,40] Thus, the dark-field image of cells that use the distinct scattering properties of gold nanostructures is a very promising tool for cellular imaging.

By using the strong optical absorption properties in the NIR region, the HGNS(Fe_3O_4@Au)/anti-HER2 were used for targeted cancer therapy of SKBR3 cells. After incubating the SKBR3 cells with HGNS(Fe_3O_4@Au)/anti-HER2, we exposed the cells (5.5×10^5–1.0×10^6 cells per mL, in 24-well plates) to an NIR laser (808 nm). Two important control experiment revealed the toxicity limits of both the laser power and the nanoparticle concentration on the HGNS(Fe_3O_4@Au)/anti-HER2-treated SKBR3 cells and the SKBR3 cells alone. When the laser power was greater than 12.68 W cm^{-2}, cell damage began to appear within 3 min, even in SKBR3 cells that had no NIR absorbing nanoparticles. Likewise, when the concentration of HGNS(Fe_3O_4@Au)/anti-HER2 reached a certain value (optical extinction density (OD) = 3.5, at 808 nm), the SKBR3 cells that were incubated with the nanoparticles for 48 h, started to be damaged without NIR photothermal therapy (see Figure S2). However, when we fixed the concentration of nanoparticles below this limit (as measured with an optical density value in an absorption spectrum, where OD = 2.0 at 808 nm), damage began to appear in the targeted SKBR3 cells with HGNS(Fe_3O_4@Au)/anti-HER2 after 3 min of lower-powered laser illumination (808 nm, 4.34 W cm^{-2}). As shown in Figure 6B, the SKBR3 cells that were targeted with HGNS(Fe_3O_4@Au)/anti-HER2 were destroyed selectively only in the region that was illuminated by the NIR laser. In contrast, no damage was observed in SKBR3 cell lines where no NIR-absorbing nanoparticles were present (Figure 6A). This result thus demonstrates that the multifunctional gold nanostructures that were developed in this study, can be used for the targeted therapy of cancer cells through the conjugation of cancer-specific biomarkers and the subsequent NIR-light illumination.

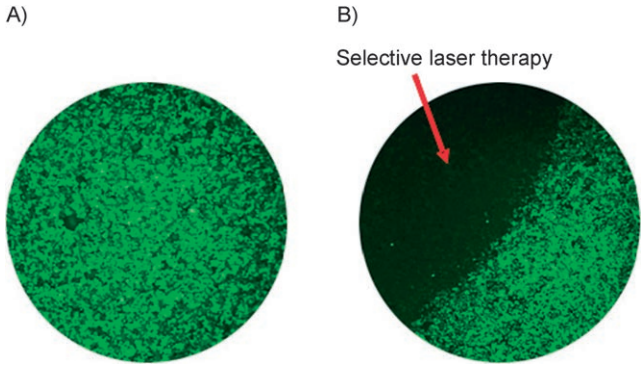

Figure 6. Fluorescence image of A) SKBR3 cells only, B) SKBR3 cells that were incubated with HGNS(Fe_3O_4@Au)/anti-HER2. After incubation, the cells were illuminated with 808 nm NIR laser (4.34 W cm^{-2}) and subsequently stained with Calcein-AM. Selective destruction was observed only in the SKBR3 cells that were targeted with HGNS(Fe_3O_4@Au)/anti-HER2.

In summary, we synthesized a novel nanostructure that has NIR-absorbing (and scattering) optical characteristics and magnetic-responsive moieties for MRI. The nanocomposite particles were successfully demonstrated for use as bimodal-imaging contrast agents as well as photonic-based therapeutic agents for cancer cells. As a perspective of this research, we expect that these nanocomposite particles would enable biologists or medical doctors to gather diagnostic in vivo imaging data by using MRI at the preoperative stage. In addition, the pathologists can directly analyze biopsy samples during the operative and postoperative stages by using the strong scattering properties in the NIR region, even without any further need to prepare additional samples. Furthermore, the multifunctional nanostructure that was developed in this research has potential in a wider variety of novel applications that are related to modulated drug delivery,[41] combined therapy (gene therapy and chemotherapy),[42] and theranostic nanoplatforms.[43]

Experimental Section

Materials: Iron(III) acetylacetonate ($Fe(acac)_3$, 99.9%), hexadecane-1,2-diol ($C_{14}H_{29}CH(OH)CH_2(OH)$, 90%), oleylamine (OAM, $C_9H_{18}{=}C_9H_{17}NH_2$, 70%), oleic acid (OA, $C_9H_{18}{=}C_8H_{15}COOH$, 99%), benzyl ether ($C_{14}H_{14}O$, 99%), mercaptoundecanoic acid (MUA, $SHC_{11}H_{22}CO_2H$, 95%), polyvinylpyrrolidone (PVP), chloroauric acid ($HAuCl_4$), and methanol were purchased from Aldrich. Gold acetate ($Au(OOCCH_3)_3$, or $Au(ac)_3$, 99.9%) was purchased from Alfa Aesar

 © 2007 Wiley-VCH Verlag GmbH & Co. KGaA, Weinheim

(Karlsruhe, Germany). Anti-HER2 (9G6, mouse monoclonal IgG_1) was purchased from Santa Cruz Biotechnology (USA). Anti-rabbit IgG-TRITC was purchased from Sigma.

Synthesis of gold-coated iron oxide nanoparticles: $Fe(acac)_3$ (0.51 g, 1.44 mmol) was mixed with oleic acid (1.5 mL, 4.5 mmol) and oleylamine (1.6 mL, 3.2 mmol) in benzyl ether (16 mL) under an argon atmosphere. After vigorous stirring, hexadecane-1,2-diol (1.65 g, 6.4 mmol) was added to the solution, and the solution was heated to 200 °C for 3 h. The solutions were further refluxed at 290 °C for 1.5 h. After cooling to room temperature, ethanol was added into the solution. A dark-brown precipitate (Fe_3O_4) was separated with a magnetic bar, and was washed with ethanol. To synthesize gold-coated iron oxide nanoparticles (Fe_3O_4@Au), the Fe_3O_4 nanoparticles (0.1 g) were dispersed in benzyl ether (40 mL). $Au(OOCCH_3)_3$ (0.7 g, 2.2 mmol), hexadecane-1,2-diol (3.1 g, 12 mmol), oleic acid (0.5 mL, 1.5 mmol), and oleylamine (3 mL, 6 mmol) were added to a phenyl ether (40 mL) solution that contained Fe_3O_4 nanoparticles. In this case, the molar ratio of gold precursor-to-iron oxide nanoparticles was approximately 7:1. Under an argon atmosphere and vigorous stirring, the solution was heated to 190 °C at 10 °C min^{-1}, then the solution was kept at 190 °C for 1.5 h. After the solution had cooled to room temperature, ethanol was added to the solution. A dark-purple material was precipitated and separated by using a magnetic bar. The precipitated product was washed with ethanol, and dispersed in hexane (100 mL) that contained oleic acid (75 mM) and oleylamine (75 mM). The nanoparticle solution appeared dark purple.

Silver-coated Fe_3O_4@Au nanoparticles: MUA (10 mM) was added into the hexane solution that contained Fe_3O_4@Au nanoparticles and the solution was sonicated for 1 h. The precipitated product was washed with ethanol and redispersed in distilled water (100 mL). The pH of the solution was adjusted to 10 by using NaOH (100 mM) after it had already been diluted 10× with distilled water. Then, 100 mM $AgNO_3$ (0.5 mL) was added and reacted at 100 °C with vigorous stirring and refluxing. After adding 50 mM sodium citrate (1 mL), the solution was further reacted for 20 min.

Hollow-type gold nanoshells that contain gold-coated iron oxide nanoparticles: After ultracentrifugation of the synthesized silver-coated Fe_3O_4@Au nanoparticles solutions 3 times at 10000 rpm, the nanoparticle solution was redispersed in distilled water (10 mL) that contained PVP (100 mg). The solutions were reacted at 100 °C for 1 h and 10 mM $HAuCl_4$ (0.8 mL) was injected at a flow rate of 0.425 mL min^{-1}. The solutions were then cooled to room temperature after 20 min reaction. NaCl (10 mL) was added, which caused a white precipitate to form; this was removed, and the final hollow-type gold nanoshells that contained iron oxide nanoparticles (HGNS(Fe_3O_4@Au)) were separated from the solution after more than 3 cycles of washing and centrifugation.

Characterization: Spectroscopic observations were made by using UV/visible–NIR spectroscopy (DU 800 spectrophotometer, Beckman Coulter, Fullerton, USA). The TEM images were obtained by using a EF-TEM (EM 912 Omega; Zeiss). Magnetic measurements were performed by using a SQUID magnetometer at 300 K (MPMS5, Quantum Design). T_2-weighted images of HGNS(Fe_3O_4@Au) (Figure S1) were obtained by an MRI scanner (1.5 T, Philips Medical system, Best, the Netherlands, Section thickness 2 mm, Matrix 192×256, Number of acquisitions: 6, FOV 100×100).

Surface modification of nanoparticles: The HGNS(Fe_3O_4@Au) were dispersed in PBS (1 mL, pH 7.4) medium and the final concentration was matched to OD = 2.8. Thiol-protein G (100 μL, 300 mg mL^{-1}) was added and the dispersion was stirred gently at 4 °C for 12 h. Then, anti-HER2 (80 μL, 200 mg mL^{-1}) was added, and the dispersion was allowed to react at 4 °C for another 12 h. Thiol–PEG (100 μL, 10 mg mL^{-1}) was then added, the dispersion was allowed to react at 4 °C for another 12 h.

Cellular imaging: The HER2-positive breast cancer cells (SKBR3, 2.5×10^5) and HER2-negative breast cancer cells (MCF7, 2.5×10^5) were prepared in 24-well plates. To visualize the attachment of the nanoparticles on the surface of each cell line, anti-rabbit IgG (TRITC) was also conjugated to the HGNS(Fe_3O_4@Au)/anti-HER2 in the antibody conjugation step. DPBS (Dulbecco's phosphate buffered saline, 500 μL, 1X, GIBCO) was used to wash the SKBR3 and MCF7 cells before experiments. Then, the HGNS(Fe_3O_4@Au)/anti-HER2 (350 μL, OD = 2.0) was added to the SKBR3 and MCF7 cells, and they were incubated at 37 °C for 1 h. After washing with DPBS (3×500 μL) to remove unattached nanoparticles, McCoy's 5A medium (300 μL, that contained 10% FBS 1X Antibiotics, GIBCO) was added. The interaction of HGNS(Fe_3O_4@Au)/anti-HER2 with each cell line was observed by using TRITC fluorescence. The light-scattering image of the SKBR3 cells that were targeted with HGNS-(Fe_3O_4@Au)/anti-HER2 was detected with an inverted microscope (Nikon) where the narrow beam of light from the tungsten source was delivered with a dark-field condenser. Only the scattered light from samples was collected by using a 100×/1.35 oil Iris objective (Uplanapo). An MRI scanner (1.5 T, Philips Medical system, Best, the Netherlands) was used for MRI and T_2-weighted image parameters were as follows: TR = 4000 ms and TE = 120, 240, 360, 480 ms, Section thickness 2 mm, Matrix 192×256, Number of acquisitions = 6, FOV = 100×100. The relaxivities were obtained from linear fitting of the $1/T_2$ vs. concentration of iron plots.

Photothermal therapy of SKBR3 cells targeted with nanoparticles: The toxicity of HGNS(Fe_3O_4@Au)/anti-HER2 was tested by incubating various concentrations of the nanoparticles with SKBR3 cells for 48 h. The cultured SKBR3 cell lines (with or without nanoparticle loading) were irradiated by using a NIR laser (Unique Mode GmbH (Gilching, Germany) diode laser module, 808 nm, optical cable designed for 200 μm, N.A. = 0.2, fiber) and remained in the culture medium for 2 h at 37 °C. After the illumination of targeted SKBR3 cells with HGNS(Fe_3O_4@Au)/anti-HER2 with the NIR laser (808 nm, 4.34 W cm^{-2}) for 3 min, the viability of the NIR-treated cells was observed by a fluorescence microscope after staining with Calcein-AM (0.1 mM).

Acknowledgements

The authors acknowledge the financial support from the KRIBB Research Initiative Program, the Regional Technology Innovation Program of the Ministry of Commerce, Industry and Energy (MOCIE), and by a grant (07142KFDA765) from Korea Food & Drug Administration in 2007.

Keywords: gold · imaging agents · magnetic properties · nanostructures · targeted cancer therapy

[1] E. J. Furlani, E. P. Furlani, *J. Magn. Magn. Mater.* **2007**, *312*, 187.
[2] J. Kim, S. Park, J. E. Lee, S. M. Jin, J. H. Lee, I. S. Lee, I. Yang, J. S. Kim, S. K. Kim, M. H. Cho, T. Hyeon, *Angew. Chem.* **2006**, *118*, 7918; *Angew. Chem. Int. Ed.* **2006**, *45*, 7754.
[3] R. Kopelman, Y. E. Lee Koo, M. Philbert, B. A. Moffat, G. Ramachandra Reddy, P. McConville, D. E. Hall, T. L. Chenevert, M. S. Bhojani, S. M. Buck, A. Rehemtulla, B. D. Ross, *J. Magn. Magn. Mater.* **2005**, *293*, 404.

 © 2007 Wiley-VCH Verlag GmbH & Co. KGaA, Weinheim

[4] L. Levy, Y. Sahoo, K. S. Kim, E. J. Bergey, P. N. Prasad, *Chem. Mater.* **2002**, *14*, 3715.
[5] W. B. Tan, Y. Zhang, *Adv. Mater.* **2005**, *17*, 2375.
[6] O. Veiseh, C. Sun, J. Gunn, N. Kohler, P. Gabikian, D. Lee, N. Bhattarai, R. Ellenbogen, R. Sze, A. Hallahan, J. Olson, M. Zhang, *Nano Lett.* **2005**, *5*, 1003.
[7] T. J. Yoon, J. S. Kim, B. G. Kim, K. N. Yu, M. H. Cho, J. K. Lee, *Angew. Chem.* **2005**, *117*, 1092; *Angew. Chem. Int. Ed.* **2005**, *44*, 1068.
[8] X. Ji, R. Shao, A. M. Elliott, R. Jason Stafford, E. Esparza-Coss, J. A. Bankson, G. Liang, Z. P. Luo, K. Park, J. T. Markert, C. Li, *J. Phys. Chem. C* **2007**, *111*, 6245.
[9] C. H. Su, H. S. Sheu, C. Y. Lin, C. C. Huang, Y. W. Lo, Y. C. Pu, J. C. Weng, D. B. Shieh, J. H. Chen, C. S. Yeh, *J. Am. Chem. Soc.* **2007**, *129*, 2139.
[10] C. C. Berry, A. S. G. Curtis, *J. Phys. D Appl. Phys.* **2003**, *36*.
[11] J. Dobson, *Drug Dev. Res.* **2006**, *67*, 55.
[12] J. Lim, R. D. Tilton, A. Eggeman, S. A. Majetich, *J. Magn. Magn. Mater.* **2007**, *311*, 78.
[13] Y. T. Lim, K. Y. Lee, K. Lee, B. H. Chung, *Biochem. Biophys. Res. Commun.* **2006**, *344*, 926.
[14] T. Osaka, T. Matsunaga, T. Nakanishi, A. Arakaki, D. Niwa, H. Iida, *Anal. Bioanal. Chem.* **2006**, *384*, 593.
[15] A. Bjørnerud, L. Johansson, *NMR Biomed.* **2004**, *17*, 465.
[16] B. Bonnemain, *J. Drug Targeting* **1998**, *6*, 167.
[17] T. Neuberger, B. Schopf, H. Hofmann, M. Hofmann, B. Von Rechenberg, *J. Magn. Magn. Mater.* **2005**, *293*, 483.
[18] G. Saini, D. Shenoy, D. K. Nagesha, R. Kautz, S. Sridhar, M. Amiji, *2005 NSTI Nanotechnology Conference and Trade Show—NSTI Nanotech 2005 Technical Proceedings* **2005**, 328.
[19] S. Eustis, M. A. El-Sayed, *Chem. Soc. Rev.* **2006**, *35*, 209.
[20] B. Khlebtsov, V. Zharov, A. Melnikov, V. Tuchin, N. Khlebtsov, *Nanotechnology* **2006**, *17*, 5167.
[21] V. P. Zharov, K. E. Mercer, E. N. Galitovskaya, M. S. Smeltzer, *Biophys. J.* **2006**, *90*, 619.
[22] L. R. Hirsch, A. M. Gobin, A. R. Lowery, F. Tam, R. A. Drezek, N. J. Halas, J. L. West, *Ann. Biomed. Eng.* **2006**, *34*, 15.
[23] L. R. Hirsch, R. J. Stafford, J. A. Bankson, S. R. Sershen, B. Rivera, R. E. Price, J. D. Hazle, N. J. Halas, J. L. West, *Proc. Natl. Acad. Sci. USA* **2003**, *100*, 13549.
[24] C. Loo, A. Lin, L. Hirsch, M. H. Lee, J. Barton, N. Halas, J. West, R. Drezek, *Technol. Cancer Res. Treat.* **2004**, *3*, 33.
[25] C. Loo, A. Lowery, N. Halas, J. West, R. Drezek, *Nano Lett.* **2005**, *5*, 709.
[26] I. H. El-Sayed, X. Huang, M. A. El-Sayed, *Cancer Lett.* **2006**, *239*, 129.
[27] X. Huang, I. H. El-Sayed, W. Qian, M. A. El-Sayed, *J. Am. Chem. Soc.* **2006**, *128*, 2115.
[28] X. Huang, P. K. Jain, I. H. El-Sayed, M. A. El-Sayed, *Photochem. Photobiol.* **2006**, *82*, 412.
[29] S. Link, M. A. El-Sayed, *Int. Rev. Phys. Chem.* **2000**, *19*, 409.
[30] J. Chen, D. Wang, J. Xi, L. Au, A. Siekkinen, A. Warsen, Z. Y. Li, H. Zhang, Y. Xia, X. Li, *Nano Lett.* **2007**, *7*, 1318.
[31] W. Cai, D. W. Shin, K. Chen, O. Gheysens, Q. Cao, S. X. Wang, S. S. Gambhir, X. Chen, *Nano Lett.* **2006**, *6*, 669.
[32] S. Kim, Y. T. Lim, E. G. Soltesz, A. M. De Grand, J. Lee, A. Nakayama, J. A. Parker, T. Mihaljevic, R. G. Laurence, D. M. Dor, L. H. Cohn, M. G. Bawendi, J. V. Frangioni, *Nat. Biotechnol.* **2004**, *22*, 93.
[33] L. Wang, J. Luo, Q. Fan, M. Suzuki, I. S. Suzuki, M. H. Engelhard, Y. Lin, N. Kim, J. Q. Wang, C. J. Zhong, *J. Phys. Chem. B* **2005**, *109*, 21593.
[34] J. Chen, J. M. McLellan, A. Siekkinen, Y. Xiong, Z. Y. Li, Y. Xia, *J. Am. Chem. Soc.* **2006**, *128*, 14776.
[35] J. Chen, B. Wiley, Z. Y. Li, D. Campbell, F. Saeki, H. Cang, L. Au, J. Lee, X. Li, Y. Xia, *Adv. Mater.* **2005**, *17*, 2255.
[36] J. M. Lee, H. K. Park, Y. Jung, J. K. Kim, S. O. Jung, B. H. Chung, *Anal. Chem.* **2007**, *79*, 2680.
[37] R. D. Averitt, S. L. Westcott, N. J. Halas, *J. Opt. Soc. Am. B* **1999**, *16*, 1824.
[38] S. J. Oldenburg, G. D. Hale, J. B. Jackson, N. J. Halas, *Appl. Phys. Lett.* **1999**, *75*, 1063.
[39] K. Aslan, J. R. Lakowicz, C. D. Geddes, *Current Opin. Chem. Biol.* **2005**, *9*, 538.
[40] X. Michalet, F. F. Pinaud, L. A. Bentolila, J. M. Tsay, S. Doose, J. J. Li, G. Sundaresan, A. M. Wu, S. S. Gambhir, S. Weiss, *Science* **2005**, *307*, 538.
[41] S. R. Sershen, S. L. Westcott, N. J. Halas, J. L. West, *J. Biomed. Mater. Res.* **2000**, *51*, 293.
[42] M. Everts, V. Saini, J. L. Leddon, R. J. Kok, M. Stoff-Khalili, M. A. Preuss, C. L. Millican, G. Perkins, J. M. Brown, H. Bagaria, D. E. Nikles, D. T. Johnson, V. P. Zharov, D. T. Curiel, *Nano Lett.* **2006**, *6*, 587.
[43] J. R. McCarthy, F. A. Jaffer, R. Weissleder, *Small* **2006**, *2*, 983.

Received: July 25, 2007
Published online on October 24, 2007

 © 2007 Wiley-VCH Verlag GmbH & Co. KGaA, Weinheim